Adaptive Toolpath

Enhanced Design and Process Control for Robotic 3DCP

Breseghello, Luca; Naboni, Roberto

Published in:
Computer-Aided Architectural Design. Design Imperatives

DOI:
10.1007/978-981-19-1280-1_19

Publication date:
2022

Document version:
Accepted manuscript

Citation for pulished version (APA):
Breseghello, L., & Naboni, R. (2022). Adaptive Toolpath: Enhanced Design and Process Control for Robotic 3DCP. In D. Gerber, E. Pantazis, B. Bogosian, A. Nahmad, & C. Miltiadis (Eds.), *Computer-Aided Architectural Design. Design Imperatives: The Future is Now - 19th International Conference, CAAD Futures 2021, Selected Papers* (pp. 301-316). Springer. https://doi.org/10.1007/978-981-19-1280-1_19

Adaptive Toolpath: Enhanced Design and Process Control for Robotic 3DCP

Luca Breseghello[1] and Roberto Naboni[1]

[1]CREATE - University of Southern Denmark, Section for Civil and Architectural Engineering

ron@sdu.dk

Abstract. The recent advances in 3D Concrete Printing (3DCP) greatly impact architectural design, highlighting the disconnection between digital modelling and manufacturing processes. Conventional digital design tools present limitations in the description of a volumetric object, which is constrained to the definition of idealized external boundaries but neglect material, textural, and machinic information. However, 3DCP is based on material extrusion following a programmed toolpath, which requires custom modelling and methods to anticipate the manufacturing results. The paper presents the development of an interactive tool for the preview of 3D printing toolpaths within Grasshopper. Through an experimental campaign and analysis of material results, we integrate geometric, physical and design feedback within the design process. The accurate control of manufacturing variables such as printing speed and dimensions of the layers, together with the simulation and visualization of the results, makes them design parameters, opening to new formal and structural articulations in the design process. The developed instruments are tested on full scale printed prototypes, where their precision is demonstrated. Integrated into a 3DCP-specific design framework, the overall approach contributes to closing the existing gap between the digital environment and fabrication procedures in the construction industry.

Keywords: Toolpath Planning, Live-physics Simulation, 3D Concrete Printing, Robotic Fabrication.

1 Introduction

3D Concrete Printing (3DCP) is a rapidly expanding field both in research and in construction practice. The newly developed technology offers disruptive potential for concrete architecture, promising geometric freedom, reduced material consumption, automation, and a shorter construction chain. Due to its recent introduction, most of its features are yet to be fully exploited, mainly due to material limitations [1], and to a process that is still experimental [2]. In 3DCP, both the manufacturing resolution and the geometrical features of printed artefacts are subject to limitations. This is due to material and technological constraints: (i) the reduced mechanical properties of concrete at its semifluid state make it challenging to print overhanging geometries;

(ii) the requirement for a continuous toolpath due to the lack of technological advances in most extrusion systems; (iii) the high dependency of the printed results on the specific material mix and environmental characteristics. Because of these restraints, the design for 3DCP has been severely limited to simplistic outcomes, which are poorly delivered on the premises of highly controllable manufacturing. While most of the current research is dedicated to fundamental material developments and technological advancements [3], little literature exists to date regarding modelling and simulation tools that allow the accounting of the material complexities during the design phase.

This research is aimed at developing a computational tool for interactive 3D modelling, simulation, visualisation and robot-code generation for robotic 3D Concrete Printing (3DCP) [4]. This tool is developed for the parametric environment of Grasshopper for Rhinoceros, and allows to (i) predict accurately the geometric characteristic of a printed concrete filament (Fig. 1); (ii) simulate the printing results of complex material behaviour, taking into account the effect of gravity and the effect of its viscosity; (iii) visualize complex printed formations and generate 3D models for further numerical analysis.

Fig. 1. Robotic 3D Printing process of test specimens for the analysis of printing parameters.

2 Related Research

Every layered AM process is characterized by the discretization of a digital 3D model into layers to generate a machining tool path. This operation is usually performed by extracting horizontal slices from a model at predefined height intervals. Standard 3D printing is performed by using external software to the design environment, namely slicer, which provides the fundamental printing information with a specific machine configuration. Well-established Fused Deposition Modelling (FDM) rely on slicing software, e.g. Cura [5], Simplify3D [6], Slic3r [7], which provides control on a large set of parameters for an automated setup and tuning of the slicing and printing phases, including the visualization of the manufacturing process. The numerous options available allow, for example, to approach the manufacturing of very different objects, use diverse materials, and tailor the printing setup to fit specific needs.

In 3DCP the effects of material and scale affect the printing results in different ways, and their inter-relationships are often the cause of unforeseen failures due to limited dimensional accuracy or mechanical performance [8, 9]. Consequently, 3DCP requires custom design strategies for specific manufacturing and material processes [10, 11]. Recent research has investigated developing software for controlling the printing process with different approaches. The first group of works aim at planning the printing process through a user-friendly slicer similar to FDM software: the Dutch-based company Vertico developed an online slicer, Slicer XL [12], which slices in horizontal layers an uploaded file in .stl format providing a visualization of the object, the motion coordinates and optionally a GCode or RAPID code; RAPCam Concrete [13], developed by RAP Technologies, works interactively with Rhino to analyze, simulate and visualize a printing toolpath, providing collision-detection, overhangs and stability verifications. The work carried out by Comminal et al. [14] exploits the Computational Fluid Dynamics (CFD) software Flow3D and validates the developed model through an experiment that compares the section of the simulation and performed tests. Another group of works looked into the integration of FE Analysis as a verification method for early-age behaviour of the printing process: Wolfs et al. [15] developed a numerical model to analyze the mechanical behaviour of early age 3D printed concrete applying the Mohr-Coulomb theory with time-dependent development of material properties and using the commercial Finite Element (FE) software Abaqus for simulation; in similar perspective, Ooms et al. [16]. Vantyghem et al. [17] developed a parametric tool in the form of a plugin ‒CobraPrint‒ for Grasshopper in Rhino that creates a FE mesh to be exported and analyzed in Abaqus for the simulation of the structural behaviour of 3D printed fresh concrete. A buckling simulation of the early age behaviour of the concrete during the printing process has been developed in Karamba within Grasshopper by Vos et al. [18]. However, most of these tools require high computing power, integration of software external to the design environment, or otherwise lack an accurate calculation and visualization of the material and layer behaviour able to provide an agile visualization of the print toolpath for controlled high-resolution printed objects.

3 Methods

An accurate representation of the 3DCP process and results requires a series of data to be gathered, analysed, and integrated. The dimension of the section of the printed filament is determined by a series of design and fabrication parameters. The paper presents a first experiment that investigates the relation between printing speed, layer height and width. The gathered data is then interpolated and implemented into a computational framework that provides a geometric representation of the printed material. Finally, a physics-based simulation is implemented within the same design environment, providing an understanding of the material behaviour and its impact on the design outcome.

3.1 Fabrication Setup

The experiments were performed using the 3DCP robotic fabrication facility of CREATE Lab at the University of Southern Denmark, consisting of an ABB 6650S industrial robot, a control unit, and an extrusion system composed of a conveying pump and a printing head with a circular nozzle diameter of 25 mm (Fig. 2). The employed cementitious material is based on a commercial product for shotcrete with aggregates with a particle size of 2 mm. Admixtures are added to control the curing time and a small dosage of polypropylene fibres. The system is based on a batch-mixing process, where the accelerating admixture is added to the mixer. This process provides a constant material composition but defines a characteristic printing timeframe where the material has mechanical resistance for buildability and the capacity to flow through the pumping system. All the experiments are run adding to the premixed powder 16.5% of water, 1.5% of an accelerator with low content of calcium-chloride and 0.01% of fibres.

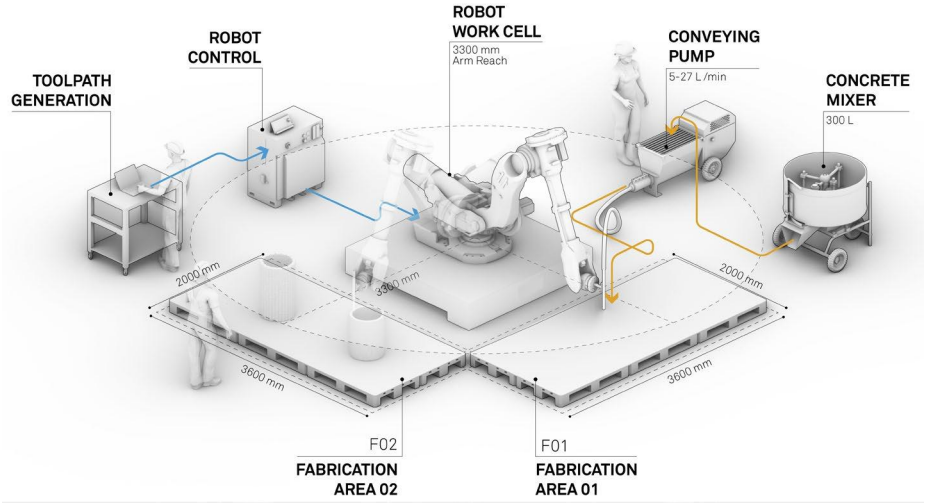

Fig. 2. 3DCP robotic fabrication setup: the robot work cell is provided with a motion code (left)and with a material feedstock (right); the setup has two fabrication areas F01 and F02.

3.2 Filament Calibration Experiment

The capacity to control the printing parameters with specific material characteristics is crucial for a successful design and fabrication with 3DCP. Therefore, a filament calibration experiment was run to investigate the resultant width *W* of a 3D printed layer and to calibrate a digital model for given ratios of printing speed *PS* and layer height *H*. These are the parameters defining the section and the volume of a printed element, assuming a fixed extrusion nozzle dimension, constant pump pressure *p* and material density, hence a constant material flow.

The experiment is based on a 500 x 500 mm custom-designed specimen, devised as a continuous print path with 100 mm spacing and five layers in height. The print path is run in an alternated fashion, i.e. the endpoint of one layer becomes the beginning of the following one with a vertical movement in height. The specific specimen design provides multiple measuring points where the speed is constant, the possibility to evaluate the influence of the movement accelerations and decelerations in longer and shorter straight segments as well as the material behaviour in the corners. For each specimen, six measurement points M_x are in the middle of each long segment, where the motion speed is constant. In addition, supplementary measures are taken to address the influence of acceleration on the robot speed. These are the points S_x, in the middle of the four short segments, and C_x, taken 30 mm from the corners on the long segments (Fig. 3).

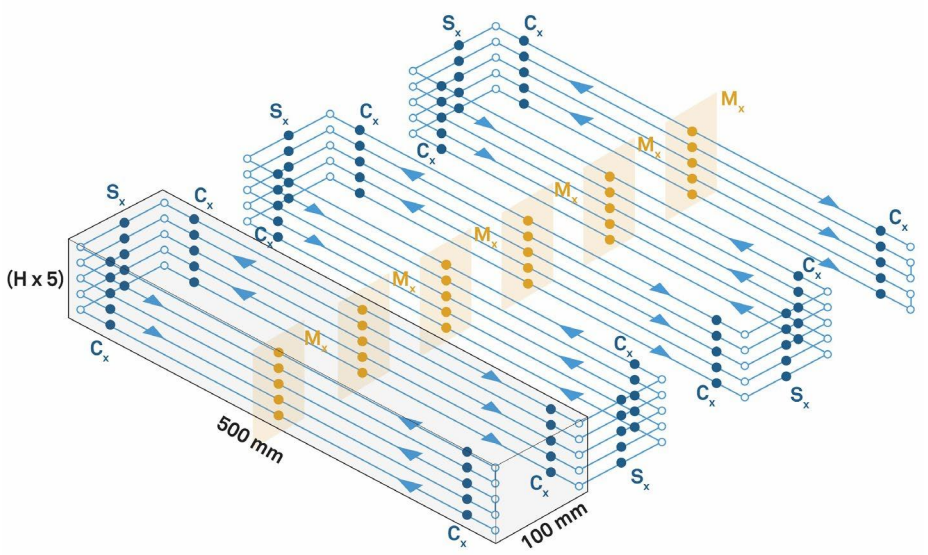

Fig. 3. Custom-design test toolpath for the evaluation of the numerical relationship between printing speed, layer height and width; each specimen is measured at the midpoint of the long segments (M_x), at the extremities of the long segments (C_x), and in the midpoint of the short segments (S_x) to account for the influence of acceleration on the printing speed.

The tested ratios between printing speed and height were chosen with a preliminary printing test. A slow movement combined with a small layer height provides a wider

section, which, if excessive, creates irregularities and uncontrolled behaviour of the deposited material. On the other hand, a fast movement and high layer reduce the filament section, with the risk of non-constant extrusion and weak adhesion between the layers. The test is performed on a matrix of printing speeds between 150 mm/s to 600 mm/s with 150 mm/s steps and layer heights from 5 mm to 25 mm with 5 mm steps, which results in 20 printed specimens.

Calibration Analysis. The print of the specimens showed (Fig. 4): *Specimen 5-150* and *5-300* produced an excess of material and an inconstant section; *Specimen 15-150* and *25-150* presented a partial collapse; similarly, specimens 15-300, 20-300, 15-450 produced a full plastic collapse during printing, due to the small printed layer width; *Specimen 10-600* had an inconstant section to the excessive printing speed. A set of specimens were not printed successfully, as the amount of material deposited was insufficient to produce a consistent layer. From a preliminary visual inspection, the print quality is lower when the speed and layer height are low. This is because an excessive amount of material is deposited and accumulated in an uncontrolled fashion; on the other hand, layers smaller than the extruder diameter present a discontinuous material distribution. The influence of the acceleration on the motion speed is visible on the specimens printed at higher speed rates. Measurements of the printed specimens are taken with an electronic calliper with tolerance ± 0.01 mm and verified through 2D scanned sections.

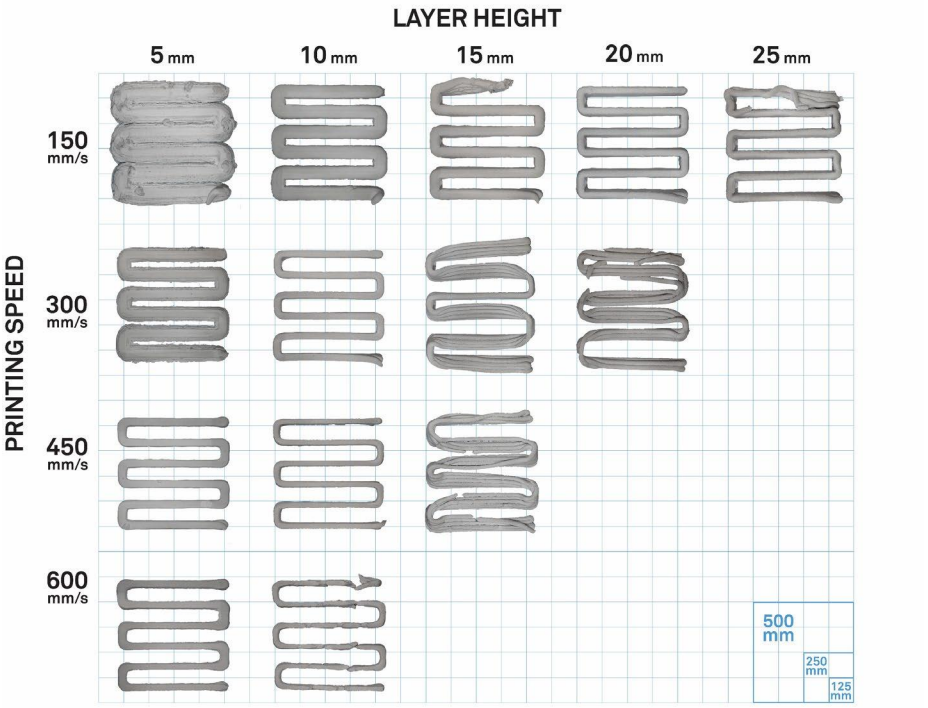

Fig. 4. Matrix of printed specimens with variable proportions of printing speed and layer height; the resultant printing width and the printing quality are evaluated.

Six sections are cut for every specimen at the middle points M_x of each long segment. These are then scanned, and the outer profile is obtained through an automated image processing routine. The sections of each specimen are then measured, overlapped, and analysed to verify the consistency between them and to formulate a geometric construction of a prototypical layer shape and dimension (Fig. 5).

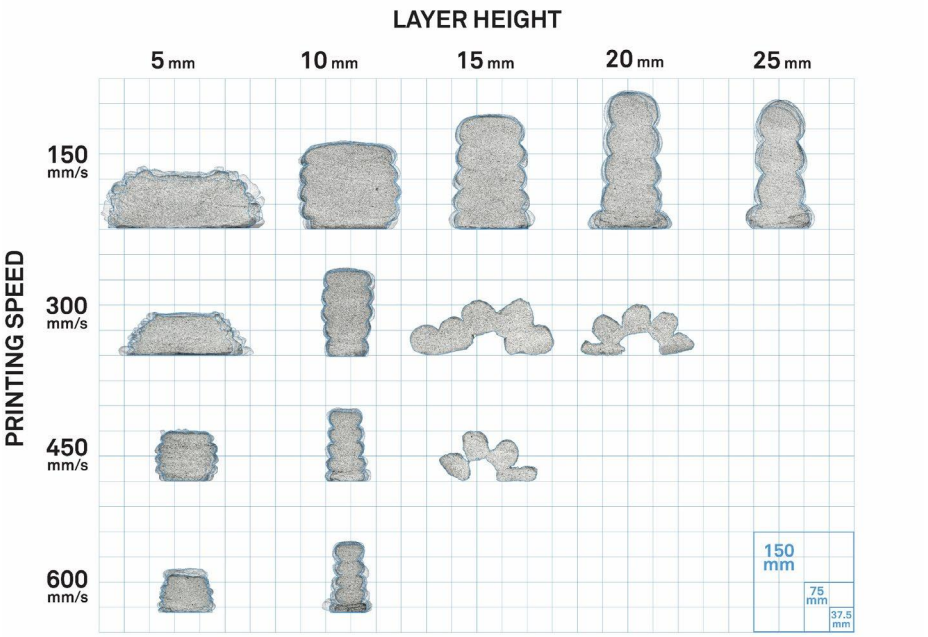

Fig. 5. Matrix of overlapped sections M_x of specimens with variable proportions of printing speed and layer height; the section dimension, their consistency, and the shape and characteristics of the layers are analysed.

Six vertices v are defined and located for each layer: four corners and the two outermost points along with the external profiles. An average for each of these points is used to determine the proportion of the average layer given a defined layer height and printing speed (Fig. 6). As the relation to the printing plane influences the dimensions of the first layer, and the last layer is not pushed from a layer above, these are disregarded from the analysis.

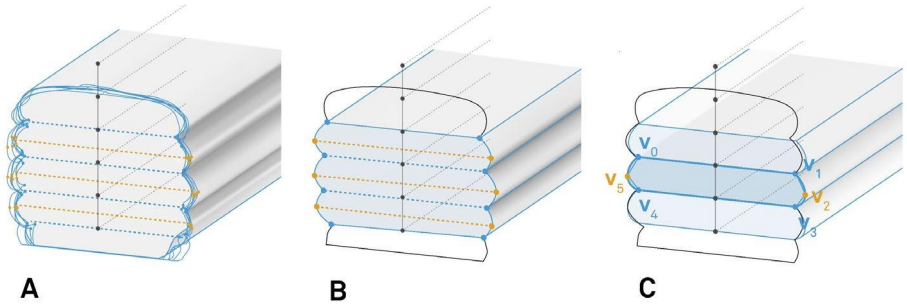

Fig. 6. Layer section analysis through (a) significant vertices *v* detection; (b) average specimen layers; (c) average layer.

As observed from the layer outline analysis, the specimens with high speed-to-height ratios present an irregular profile, both in the width of the layers in each cut section and between the different sections of the same specimen. The *Specimens 5-150* and *5-300* have an irregular profile and very little correspondence between the different cut sections, which prevent from calculating the shape of the reference layer; on the other hand, *Specimens 10-600, 15-300, 15-450* and *20-300* present discontinuous material extrusion and collapse that prevented from taking all the planned section cuts.

3.3 Modelling of Filament Geometry

When a 3D digital model is sliced into a toolpath for the layered extrusion, an approximation of the original shape is created. To address this transformation, we developed a framework from input 3D design to machine-readable code that, taking from the findings of the filament calibration experiment, integrates visualisation and simulation of the printing toolpath.

Developed in C# within Grasshopper for Rhino, the computational model takes from a toolpath generated slicing a generic input geometry, i.e. surface, BReps, meshes. In the form of polylines generated at points P_x, the toolpath slices are found at a vertical distance H_x, which defines the layer height of the print. As described in 2.2, given constant fabrication parameters, a resultant width W_x and a contact surface S_x are defined. These three parameters define a series of sections s_x, built perpendicular to the toolpath in each point P_x, by the six vertices v_x following the findings of the filament calibration experiment described in *2.2*. A low poly mesh is created through the sections and subsequently into a Subdivision Surface (SubD) object. This high precision spline provides a smooth curvilinear object representation from a polygonal mesh input (Fig. 7).

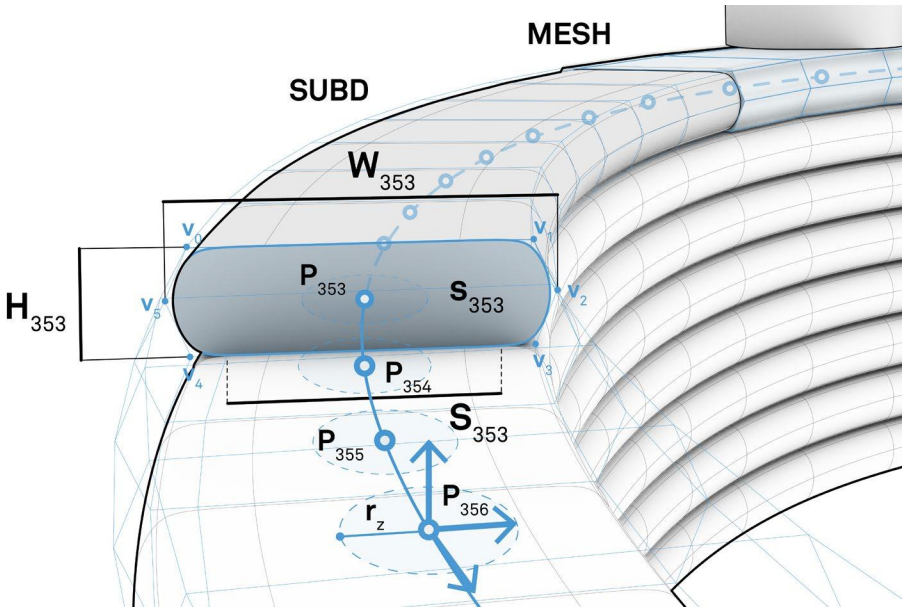

Fig. 5. Visualization of the geometric description of the layer toolpath section: generating vertices *V*, height *H*, width *W*, contact surface *S*, motion planes *P*, robot motion zone r_z.

Parallelly to the visualisation, the layer generation process outputs a set of 3D planes that will serve as motion positions for the linear movement of the robot. The distance between these points is adaptive to the local curvature of the path to minimise the number of points and maintain the closest fidelity to the input shape, and it is approximated. The generated and analysed toolpath is then translated into a RAPID module file with Robots in Grasshopper using the defined motion planes and printing parameters [19]. These are the printing speed, print zones of radius r_z, i.e. a variable that determines the distance at which the robot computes the movement to the next point, and further additional movements for the pre- and post-printing routine. Moreover, a series of quantitative data about the printing process, i.e. total printing time, layer printing time, material quantities, are defined.

The presented framework for visualization and code-generation is tested against a real-case scenario of a circular element of 400 mm circumference with regular geometry. The layers are defined by a 12 mm height and by a variable speed: along with each circular layer, the base speed of 450 mm/s was changed to 200 mm/s in seven predefined areas to increase the layer width.

3.4 Physics-based simulation for complex toolpath

The large extrusion rate and the density of the material during 3D printing with concrete create emergent behaviours that can be highly unpredictable. The visualization of the material behaviour during the deposition process is highly beneficial to predict failure. It is exploited in the design process to control the toolpath or play with emer-

gent material behaviours. A particle-based simulation integrated into the computational framework is developed taking advantage of the live-physics engine of Kangaroo in Grasshopper and here used to visualize and preview such behaviour and inform the design process (Fig. 8). The simulation is run onto the set of points and lines forming the toolpath, considering the dimensional parameters of the layer. The process considers the set of physical forces generated by the behaviour of concrete when printed. It translates them into a set of motion vectors and constraints in the digital environment. The gravity is directly reflected through a constant negative vertical force *g* that applies onto each point P_x of the toolpath; the interaction between the segments is calculated through an interaction force *i* between the points; to avoid excessive deviation of the points, a length constraint *l* is applied; to reduce the number of points needed in the simulation while keeping the semi-fluid behaviour of the cementitious material, a bending force *b* applied to consecutive lines creates a resistance mechanism reducing the occurrence of sharp angles in the polyline-based simulated path. Moreover, a loose axial constraining force *h* applied onto the points that block movements on the horizontal plane is used to avoid consecutive layers to slip and to simulate the friction occurring between them.

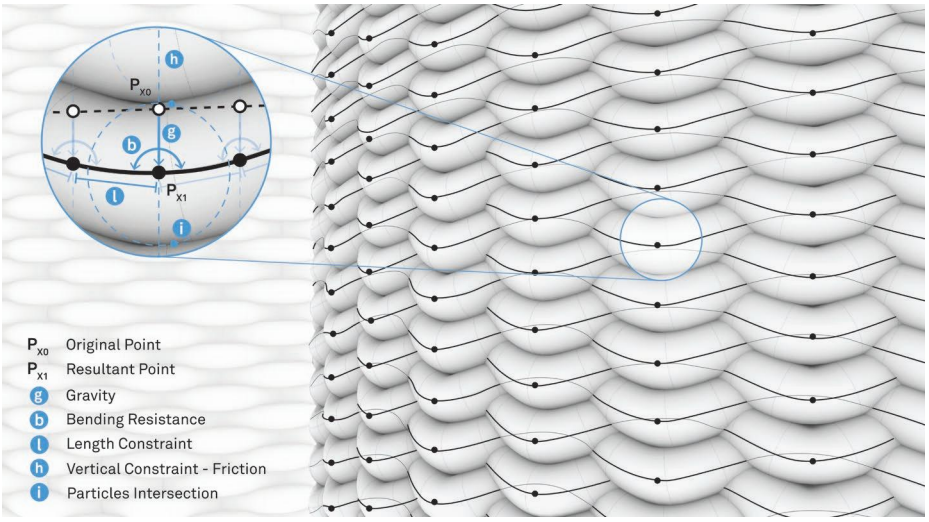

Fig. 8. Print visualization of a physics-based simulation of a patterned toolpath: a combination of forces shapes the previewed toolpath rendering the emergent behaviour of the material.

The presented simulation method is tested against a fabricated hollow circular column designed with a diameter of 400 mm and a total height of 2300 mm. Printed with a constant speed of 300 mm/s, a layer height of 10 mm, and a resulting width, the column and its pattern highlight the relevance of the emergent material behaviour during the printing process. Conceived to enhance its structural stability as well as to provide an unprecedented surface finishing, the toolpath has 230 horizontal layers characterized by a pattern with an amplitude of 150 mm at the base linearly approaching zero and a linear path at the full height of the column.

4 Results and Discussion

In this work, we introduced a modelling framework where the layered shape of the printed object and the machining toolpaths are controlled simultaneously. Taking advantage of such an approach, we generated a larger body of design opportunities through enhanced control over the appearance of the layered of the printed object and the emergent material behaviours during the printing process.

4.1 Layer Dimension Data

Results from the analysis of the resultant width from variable proportions of layer height and printing speed are plotted (Fig. 9). *Specimen 5-150* presents uneven boundaries and an average width of about 89 mm. On the other hand, *Specimen 15-450* has an average measured width of 19.8 mm, smaller than the extruder dimension. This is reflected in a discontinuous extrusion which left voids along the print path. The mean deviation for each set of M_x measures is on average 2.42 mm, increasing to 4.2 mm for wider sections where the material deposition is less controlled; *Specimen 10-300* and *Specimen 15-150* presents a deviation of less than 1 mm. The supplementary measures *S* and *C* highlight an overall section increase of about 2 mm on average, due to the acceleration and deceleration of the robot motion around the corners. For all the tested speeds, a non-linear proportion between layer height and layer width is observed. As the layer height increases, the difference in the resultant width decreases. *Specimens 25-150* and *20-150* presents an average width in the points M_x of 31.41 mm and 34.93 mm, with only 3.52 mm of difference between the two; on the other hand, the *Specimens 5-300* and *5-150* presents a difference of 26.64 mm on average.

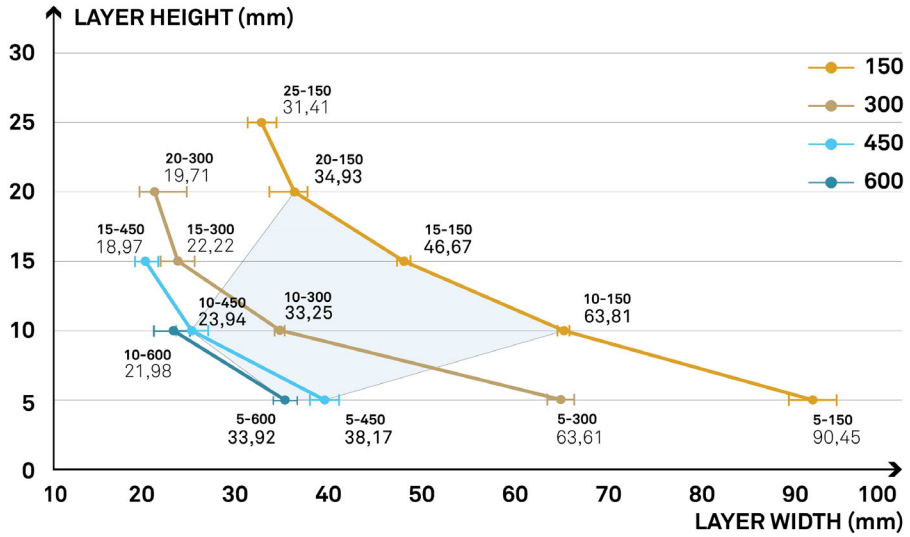

Fig. 9. Graph representation of the average resulting width from a matrix of printing speed and layer height; each width value was measured in the midpoints M_x of the long segments in the specimens.

4.2 Proof of Concept: Speed Variation

The geometric filament description developed in Section 3.3. was tested against the real-case scenario of a circular hollow column, to which variations in the sections are implemented through the variation of the printing speed. Tuned through the filament calibration results, the visualization framework previewed a variation in thickness from 53.7 mm in the thicker sections with a printing speed of 200 mm/s and about 24.1 mm. The speed was set at 450 mm/s. The printed element showed an average variation between 56.3 mm and 25.2 mm in the two extremes, i.e. areas with the lowest and highest print speed, with a resultant average deviation of 3.6 mm and 1.2 mm from the digital model (Fig. 10). However, it is to be noted that in the areas of lower printing speed, the printed object presented an irregular surface finishing due to the high rate of material extruded and the consequent pressure exerted by the printing nozzle on it.

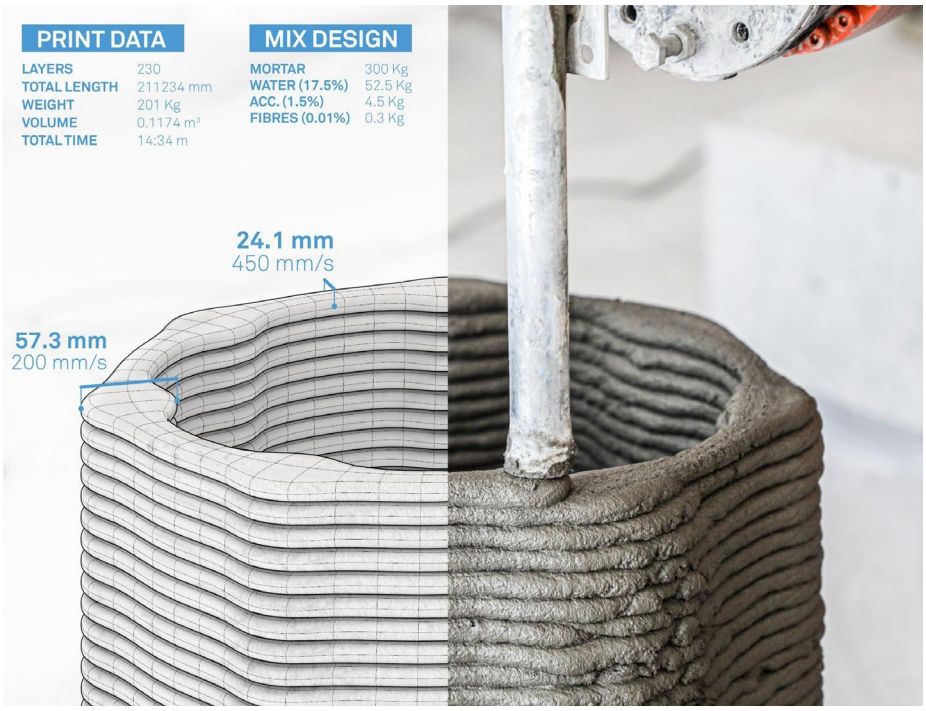

Fig. 10. Comparison of the geometric visualization of the printing process (left) and the proof-of-concept print of a circular hollow element with variable printing speed. The computational model provides data about the print and the mix design.

4.3 Proof of Concept: Woven Column

The architectural-scale hollow column is characterised by a zigzag pattern with a linearly variable amplitude that gets to a circumference at its full height. The pattern emerging from the effect of the gravity on material that is not supported from the layer below reflects the designed gradient of the toolpath: higher amplitude corresponds to a more considerable amount of material collapsing and sagging onto the layer below. Particularly in the first half of the printed element, the effect causes an interlocking mechanism of consecutive layers. Similarly, the simulation shows a gradual weaving effect (Fig. 12). This programmed design feature increased the buildability of the column during the printing process and generated a surface pattern hardly achievable with conventional concrete casting fabrication methods.

The computational model is built upon an empirical reconstruction of the physical forces observed on physical artefacts. This implies a degree of uncertainty in the model's flexibility, which will require further investigation through observation and numerical analysis of various emerging behaviours. However, the model demonstrates a relevant design tool that provides a relatively fast and reliable preview of the toolpath and the emerging effects due to material behaviour that characterize the printed artefact (Fig. 11). This allows for more rapid design iterations and the integration and exploitation of the emergent effects of the extruded concrete as design features.

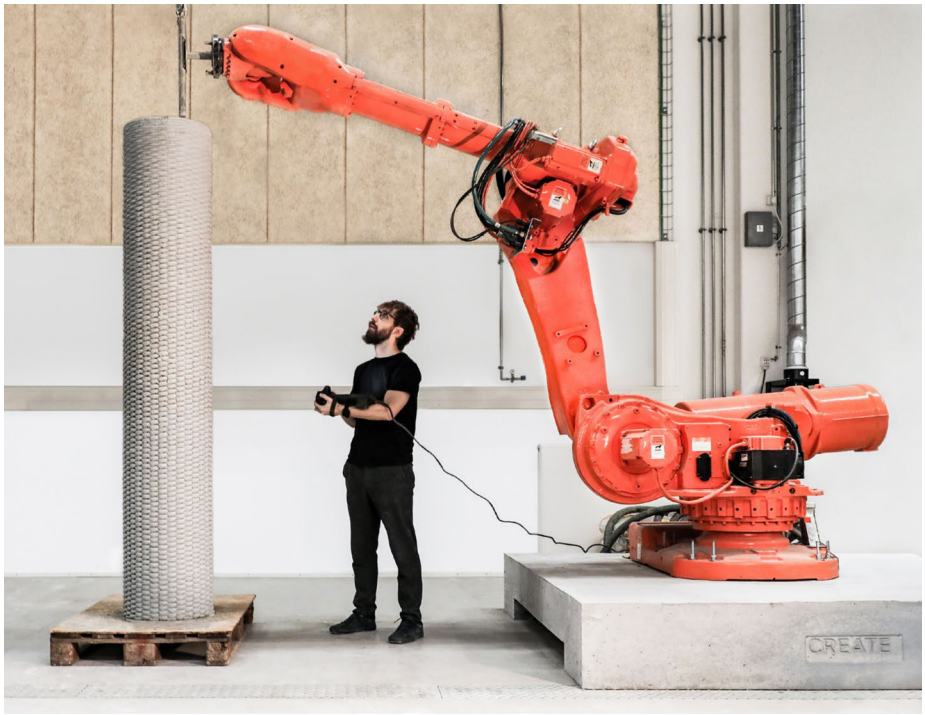

Fig. 11. Concrete 3D Printed hollow column presenting a woven toolpath with a gravity-induced deformation.

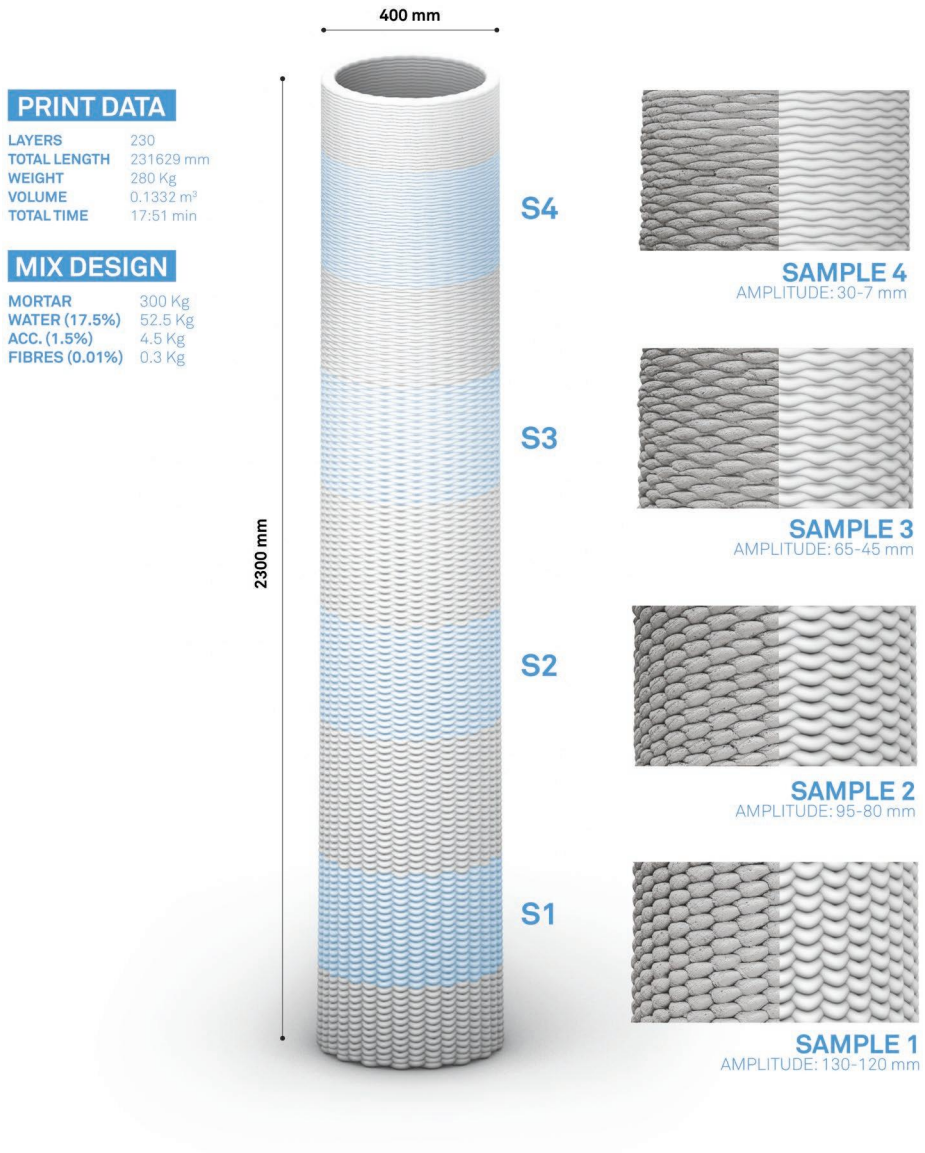

Fig. 12. Comparative visualization of the proof-of-concept column characterized by a variable-amplitude weaving pattern.

5 Conclusions

The presented experimental work addressed and exploited the design and 3D modelling paradigm shift imposed by the manufacturing process of extrusion-based 3DP. The technique imposes a new modelling approach that supports new design

affordances when compared to standard concrete casting. 3DCP offers the possibility to control the material layout in every part of an object and use highly specific material patterns informed by structural or environmental analysis. The developed computational model can integrate a series of analysis on the design and fabrication process, i.e. print overhangs, centre of mass, and curvature, developed in a parallel work by the authors [20]. The proposed approach introduces realistic means of previewing and assessing complex printing patterns. This is particularly useful whenever a non-standard printing toolpath is used in the printing of architectural objects for ornamental or structural reasons. This enhanced level of design control enables various design possibilities, as it can provide higher control on the superficial and sectional features of a 3D printed object. Such patterns can be applied to characterize the aesthetics of facade elements specifically (Fig. 13). Future works will focus on analytical methods to assess the early-age physical behaviour of printed concrete and tuning the physics-based simulation parameters. Moreover, the research will be steered to developing a real-time feedback-loop workflow to analyse the printing process, compare it to the digital model, and correct the toolpath to compensate for deviations. In parallel, the model will be tested against a series of architectural-scale prototypes, developing design strategies that take advantage of its flexibility and emergent behaviours.

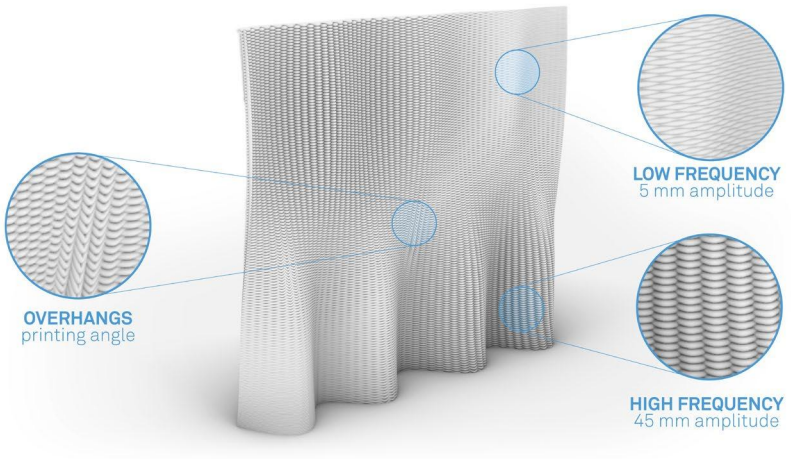

Fig. 13. Architectural outlook: a complex wall geometry and its toolpath are designed; the structure features a locally varying weaving pattern which is physically simulated to detect overhangs and visualize the emergent outlook of the planned toolpath.

Acknowledgements. This work was carried out at the CREATE Lab, a research infrastructure for digital fabrication at the University of Southern Denmark, in cooperation with Hyperion Robotics. The project has been developed with the help of Philip James Douglas, Mads Sørensen, Simon Andreasen, and students from the CREATE Summer School 2020. The authors wish to thank Weber Saint-Gobain for in-kind support of concrete material, Fosroc for in-kind support of concrete admixtures and Danish Fibres for the in-kind support of polypropylene fibers.

References

1. Roussel, N.: Rheological requirements for printable concretes, Cement and Concrete Research, 112(May), 76-85 (2018).
2. Suiker, A.S., Wolfs, R.J., Lucas, S.M. and Salet, T.A.: Elastic buckling and plastic collapse during 3D concrete printing, Cement and Concrete Research, 135(January), 106016 (2020).
3. Craveiro, F., Nazarian, S., Bartolo, H., Bartolo, P. J., & Pinto Duarte, J.: An automated system for 3D printing functionally graded concrete-based materials. Additive Manufacturing, 33(January) (2020).
4. Breseghello, L., Sanin, S. & Naboni, R.: Toolpath Simulation, Design and Manipulation in Robotic 3D Concrete Printing. In: Projections - Proceedings of the 26th International Conference of the Association for Computer-Aided Architectural Design Research in Asia, CAADRIA 2021. Globa, A., van Ameijde, J., Fingrut, A., Kim, N. & Lo, T. T. S. (eds.). Hong Kong: The Association for Computer-Aided Architectural Design Research in Asia (CAADRIA), Vol. 1. p. 623-632 (2021).
5. Cura Homepage. https://ultimaker.com/software/ultimaker-cura, last accessed 2021/02/07
6. Simplify3D Homepage, https://www.simplify3d.com/, last accessed 2021/02/07
7. Slic3r Homepage, https://slic3r.org/, last accessed 2021/02/05
8. Wolfs, R.J.M., Bos, F.P., Salet, T.A.M.: Early age mechanical behaviour of 3D printed concrete: numerical modelling and experimental testing, Cem. Concr. Res. 106, 103–116 (2018).
9. Kruger, J., Cho, S., Zeranka, S., Viljoen, C. and van Zijl, G.: 3D concrete printer parameter optimisation for high rate digital construction avoiding plastic collapse, Composites Part B: Engineering, 183(October 2019), 107660 (2020).
10. Ahmed, Z. Y., Bos, F. P., Wolfs, R. J. M., Salet, T.A.M.: Design considerations due to scale effects in 3d concrete printing. 8th International Conference of the Arab Society for Computer Aided Architectural Design, 115–124 (2016).
11. Carneau, P., Mesnil, R., Roussel, N., & Baverel, O.: An exploration of 3d printing design space inspired by masonry. Proceedings of the IASS Annual Symposium, November, 1–9 (2019).
12. slicerXL Homepage, https://www.slicerxl.com, last accessed 2021/02/01.
13. RAPCAM Concrete, https://www.raptech.io/rapcam, last accessed 2021/02/01
14. Comminal, R., Serdeczny, M. P., Ranjbar, N., Mehrali, M., Pedersen, D. B., Stang, H., & Spangenberg, J.: Advancing precision in additive manufacturing modelling of material deposition in big area additive manufacturing and 3D concrete printing. Joint Special Interest Group Meeting between Euspen and ASPE Advancing Precision in Additive Manufacturing, 151–154 (2019).
15. Wolfs, R., Bos, F.P. and Salet, T.A.: Early age mechanical behaviour of 3D printed concrete: Numerical modelling and experimental testing, Cement and Concrete Research, 106(May 2017), 103-116 (2018).
16. Ooms, T., Vantyghem, G., Van Coile, R., & De Corte, W.: A parametric modelling strategy for the numerical simulation of 3D concrete printing with complex geometries. Additive Manufacturing, 124187 (2020).
17. Vantyghem, G., Ooms, T., & De Corte, W.: VoxelPrint: A Grasshopper plug-in for voxel-based numerical simulation of concrete printing. Automation in Construction, 122(May 2020), 103469 (2021).
18. Vos, J., Wu, S., Preisinger, C., Tam, M. and Xiong Neng, N.: Buckling Simulation for 3D Printing in Fresh Concrete. Available from

https://www.karamba3d.com/examples/moderate/buckling-simulation-for-3d-printing-in-fresh-concrete (2020).
19. Soler, V. and Huyghe, V.: Robots. Available from https://github.com/visose/Robot (2016).
20. Naboni, R. and Breseghello, L.: High-Resolution Additive Formwork for Building-Scale Concrete Panels. In: F. P. Bos, S. S. Lucas, R. J. M. Wolfs, T. A. M. Salet (Eds.), Second RILEM International Conference on Concrete and Digital Fabrication - Digital Concrete 2020. DC 2020. RILEM Bookseries, 28. Springer, Cham. (2020).